Enhancement and Suppression of Vibrational Coherence in Degenerate Four-Wave-Mixing Signal Generated from Dye-Doped Polymer Films

Yutaka Nagasawa,* Yoshio Mori, Yukako Nakagawa, Hiroshi Miyasaka, and Tadashi Okada
Division of Frontier Materials Science, Graduate School of Engineering Science, and Research Center for Materials Science at Extreme Conditions, Osaka University, Toyonaka, Osaka 560-8531, Japan
Received: March 8, 2005; In Final Form: April 19, 2005

Vibrational coherence in the degenerate four-wave-mixing (DFWM) signal generated from polymer films doped with a dye, oxazine 4 (Ox4), at 10 K was investigated. It was found that the amplitudes of some low-frequency oscillations (<400 cm^{-1}) were enhanced when the delay between the first and second femtosecond pulses was set *out of phase* with the oscillation period. Frequency and reorganization energy dependence was investigated by computer simulation based on the response function formalism which considers all the possible Liouville space pathways for the DFWM signal. It was revealed that low-frequency oscillations with weak coupling to the optical transition can be enhanced in the stimulated photon echo signal compared to the transient grating signal.

1. Introduction

When the fwhm of the laser pulse is sufficiently shorter than half the period of a molecular vibration, a nuclear motion can be coherently induced by ultrafast nonlinear optical processes.[1] The recent progress in femtosecond laser techniques has enabled direct observations of such coherent vibrations in a variety of systems, from simple two-atom molecules[2−4] to large complex biomolecules.[5−7] Controlling coherent nuclear motion during chemical reaction could lead to an exclusive generation of desired products. Such a concept is generally called "coherent control" and is extensively studied.[8−10] Coherent control by multiple pulses is also applied to two-dimensional (2D) vibrational spectroscopy which is the analogue of 2D NMR.[11−13] Manifestation of multidimensional analysis has launched a revolutionary development in the field of NMR, and a similar impact is also expected for 2D vibrational spectroscopy.[14−16]

Recently, control of coherence and population transfer between the ground and excited states was reported utilizing the degenerate four-wave-mixing (DFWM) technique in the gas phase.[17,18] It was demonstrated for iodine (I_2) vapor that the coherent vibration observed in the electronic population period changed from the one in the ground state to that in the excited state depending on the delay between the first and second pulses, t_{12} (the coherent period). When the delay was set *out of phase*, $t_{12} = 2\pi(n + 1/2)/\omega_e$ ($n = 0, 1, 2, ...$), with the excited state vibration, ω_e, the signal from the ground state diminished. On the contrary, when it was set *in phase*, $t_{12} = 2\pi n/\omega_e$, the ground state signal reached a maximum.

The DFWM technique is also applied to study molecular dynamics in the condensed phase. Especially, the photon echo technique has been widely used to investigate molecular dynamics in amorphous solids and liquids.[19−24] However, electronic dephasing in the condensed phase is extremely fast at temperatures of >10 K and the photon echo signal diminishes very rapidly in the femtosecond time regime.[22,25] Therefore, coherent control by DFWM as demonstrated for I_2 vapor is extremely difficult; that is, the value of t_{12} cannot be elongated very much. To the best of our knowledge, coherent control of molecular oscillation is only accomplished as the "mode-suppression" effect in the condensed phase photon echo studies.[26−28]

When the photon echo technique is utilized to extract the pure electronic dephasing time, T_2, coherent vibration is a disturbance because it hinders the very rapid signal decay. For an inhomogeneously broadened system, with a single harmonic mode at a frequency of ω, the stimulated echo signal in the $-\boldsymbol{k}_1 + \boldsymbol{k}_2 + \boldsymbol{k}_3$ direction can be approximated as[27]

$$S(t_{12},t_{13}) \cong \exp[-4D_{vib}{}^2(1 - \cos \omega t_{12})(1 - \cos \omega t_{13})] \exp\left[-\frac{4t_{12}}{T_2}\right] \quad (1)$$

where D_{vib} is the dimensionless nuclear displacement (coupling parameter) of the mode. For mode-suppressed echo measurement, the delay between the first and third pulses, t_{13}, is set *in phase* ($2\pi n/\omega$) with the vibration and t_{12} is scanned to eliminate coherent vibration. When $t_{13} = 2\pi(n + 1/2)/\omega$, the vibration has the strongest amplitude in echo signal. However, to the best of our knowledge, enhancement of coherent vibration has never been observed. When t_{12} is scanned with t_{13} set to 0 (*in phase*), the DFWM signal becomes equivalent to the transient grating (TG) signal.[29] The above expression indicates that the amplitude of a coherent oscillation can be stronger for the stimulated photon echo signal at $t_{13} = 2\pi(n + 1/2)/\omega$ compared to that for the transient grating signal ($t_{13} = 0$). Control of coherent oscillation can be achieved even in the condensed phase, when certain conditions are fulfilled.

We have been investigating the effect of coherent vibrations on DFWM signals generated from dye-doped polymer films,[29] and in the present report, we will show that some low-frequency coherent vibrartions can be enhanced by controlling the pulse sequence. Our experiment revealed that the amplitude of the vibration actually became stronger than that observed in the TG signal ($t_{12} = 0$) when the delay was set *out of phase* for the stimulated echo signal. Interestingly, this effect was only observed for weak low-frequency vibrations at ≤ 350 cm^{-1} and not for the strong vibration at 586 cm^{-1}. de Boeij et al. have shown that eq 1 is only applicable to systems in the optical

* To whom correspondence should be addressed. E-mail: nagasawa@cobalt.chem.es.osaka-u.ac.jp.

10.1021/jp051187p CCC: $30.25
Published on Web 05/19/2005

Bloch limit.[28] Thus, a computer simulation based on the evolution of density matrix in Liouville space[30] was carried out, and it revealed that the mode-suppression and enhancement effects are more apparent for low-frequency vibrations with weak optical coupling.

2. Experimental Section

A homemade femtosecond cavity-dumped Kerr lens mode-locked chromium-doped forsterite (Cr:F) laser was utilized for the experiment. The details of the laser were reported elsewhere.[31,32] Briefly, the Cr:F laser was pumped by a diode-pumped Nd:vanadate laser (Spectra Physics Millenia IR) at 1064 nm with a 7.0 W power. The repetition rate of the cavity dumping was 100 kHz, and the output was focused into a 4 mm LBO crystal to generate second harmonic pulses centered at 635 nm. The second harmonic pulse energy was about 4 nJ/pulse, and it was divided into three beams with equal energy ($\leq$1 nJ/pulse) by beam splitters. After passing through the delay line, three beams were aligned to form an equilateral triangle and focused into the sample.[29] The relative polarizations were set parallel for all three pulses. The autocorrelation traces between all three pulses were measured by a 0.5 mm LBO crystal with the same setup as that used for the echo experiment. The amount of glass traversed by the beam was adjusted to be equal for the autocorrelation and photon echo measurements. The pulse duration was ~26 fs fwhm, assuming a Gaussian pulse.

The echo signals appearing in the phase-matching direction of $-\boldsymbol{k}_1 + \boldsymbol{k}_2 + \boldsymbol{k}_3$ and $\boldsymbol{k}_1 - \boldsymbol{k}_2 + \boldsymbol{k}_3$ were simultaneously measured by a pair of photodiodes (New Focus, model 2031) and lock-in amplifiers (EG&G Instruments, model 5210). However, in this report, signals appearing only in the direction of $-\boldsymbol{k}_1 + \boldsymbol{k}_2 + \boldsymbol{k}_3$ are presented. Most of the stimulated echo signal was measured by varying t_{12} and t_{13}, while for the temperature dependent measurement, the signal intensity was monitored as a function of t_{12} by keeping the delay between the second and third pulses constant, $t_{23} = 387$ fs.[29] The sample was kept in a closed-cycle helium gas cryostat for temperature control.

The sample was a film of oxazine 4 (Ox4)-doped poly(vinyl alcohol) (PVA) or poly(methyl methacryrate) (PMMA) with a thickness of 100−200 μm with an optical density of ~1.3. Ox4 perchlorate (Exciton), PMMA (average molecular weight ~120 000, Aldrich), and completely hydrolyzed PVA (average molecular weight ~44 000, Wako Pure Chemical Industries Ltd) were used as received. Ox4 (~2.5 mg) was dissolved in 40 mL of chloroform, and PMMA (2 g) was added into 10 mL of this solution.[29] For PVA film, a 3/2 water/ethanol binary solution was used to avoid aggregation of Ox4. The mixed solution was passed through a 0.2 μm filter and dropped onto a glass plate. The sample was dried under atmosphere for a day and then kept in a vacuum desiccator for at least a week. The sample film was removed from the glass plate after drying. Absorption spectra of the films were measured with a Hitachi U-3500 spectophotometer. The absorption band of the aggregate appears on the blue side of that of the monomer Ox4. In aqueous solution, the absorption of the monomer peaks at ~614 nm, while that of the aggregate peaks at ~570 nm. The absorption of Ox4 in PVA peaked at 624 nm, and a shoulder appeared at ~580 nm. The shoulder also appears in the computer simulated absorption spectrum, indicating a vibrational structure (see Figure 8). Even if there were some aggregates in the sample, the excitation laser wavelength was centered at ~635 nm and the signal should be arising mainly from the monomer. The absorption band of Ox4 in PMMA was similar to that in PVA, while the peak was shifted to ~610 nm.

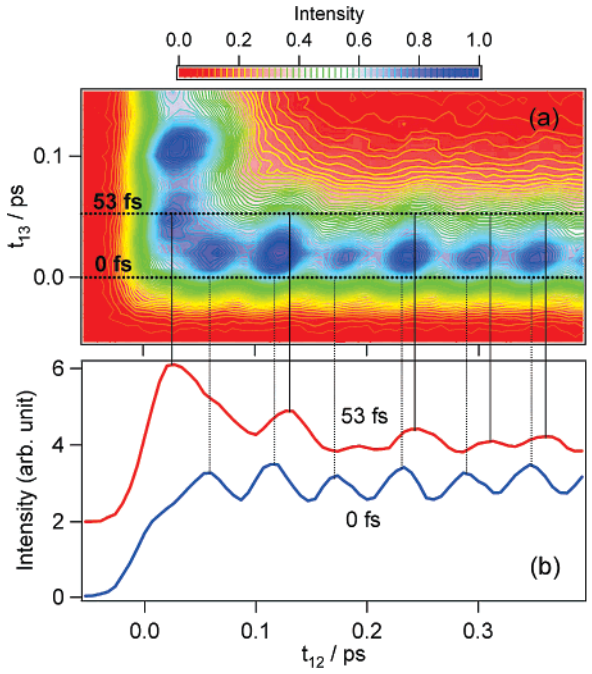

Figure 1. (a) Two-dimensional plot of the DFWM signal generated from Ox4/PVA at 10 K. (b) The t_{12} dependence of signal intensity at $t_{13} = 0$ fs and $t_{13} = 53$ fs.

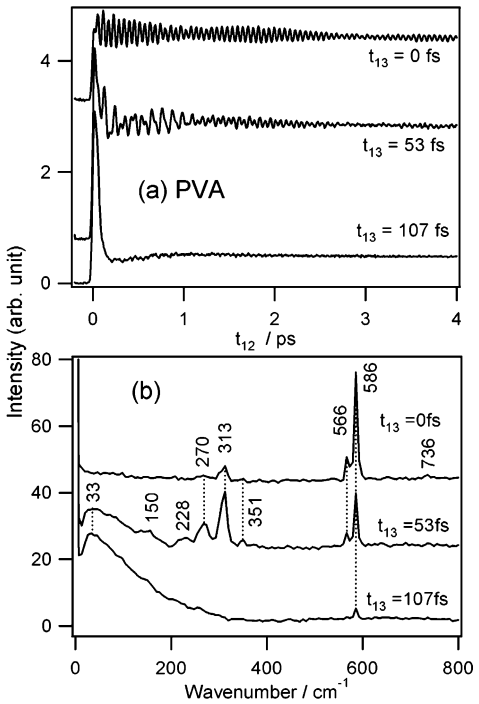

Figure 2. (a) The t_{12} dependence of the DFWM signal intensity at $t_{13} = 0$ fs, $t_{13} = 53$ fs, and $t_{13} = 107$ fs for Ox4/PVA at 10 K. (b) The real parts of the Fourier transformed spectra of the signals.

3. Results and Discussions

3.1. Experimental Results. A two-dimensional plot of the stimulated photon echo signal from Ox4/PVA at 10 K is displayed in Figure 1a. The signal intensity is plotted as a function of t_{12} and t_{13}, and the intensity is the strongest at the blue part and the weakest at the red part, respectively. Since all three pulses are equivalent, the horizontal axis (t_{12}) and the vertical axis (t_{13}) are indistinguishable and can be exchanged.[29] The strong signals along $t_{12} = 0$ and $t_{13} = 0$ are the transient grating (TG) signals generated by properly ordered pulses and

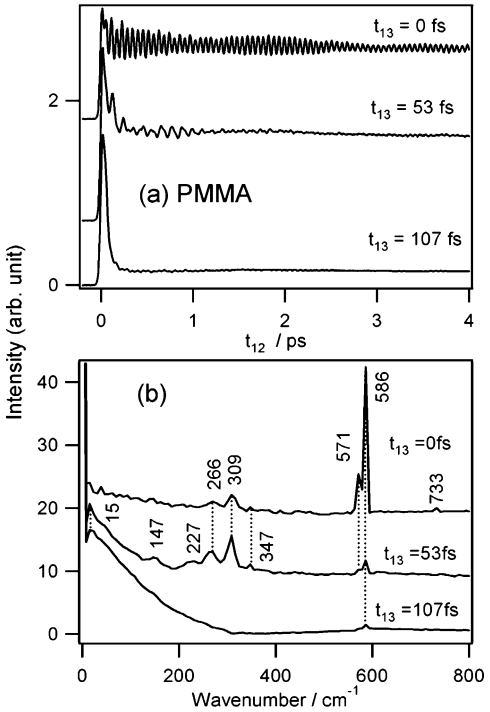

Figure 3. (a) The t_{12} dependence of the DFWM signal intensity at $t_{13} = 0$ fs, $t_{13} = 53$ fs, and $t_{13} = 107$ fs for Ox4/PMMA at 10 K. (b) The real parts of the Fourier transformed spectra of the signals.

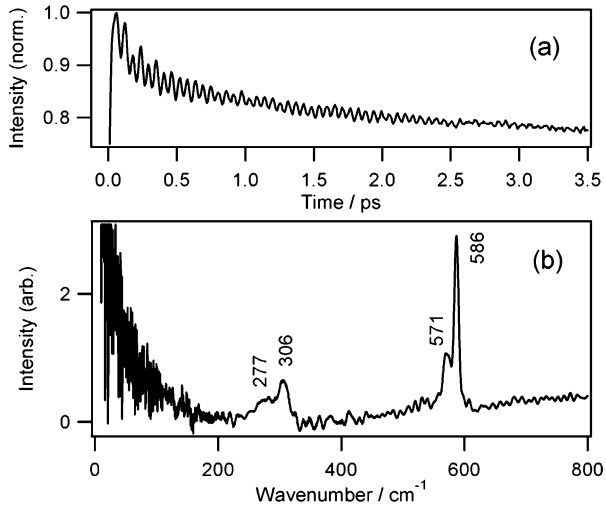

Figure 4. (a) Femtosecond pump−probe signal of Ox4 in methanol solution at room temperature. (b) The real part of the Fourier transformed spectrum of the signal. See ref 24 for details.

misordered pulses, respectively. In the case of $t_{12} = 0$, the interference pattern generated by the first and second pulses diffracts the third pulse, while, for $t_{13} = 0$, the pattern caused by the first and third pulses diffracts the second pulse. It can be seen that the signal is strongly modulated by the coherent intramolecular vibrations of Ox4. When horizontal cross sections at $t_{13} = 0$ and $t_{13} = 53$ fs are compared, it can be seen that the appearance of the coherent oscillation is rather different (Figure 1b). This feature is pronounced when t_{12} is scanned for a wider range, as shown in Figure 2a. It looks as if the signal is oscillating at a higher frequency at $t_{13} = 0$ fs than at $t_{13} = 53$ fs. At $t_{13} = 107$ fs, oscillation is almost diminished and an ultrafast decay (<100 fs) is followed by a slight recurrence.

Real parts of the Fourier transformed spectra of the echo signals are shown in Figure 2b. For $t_{13} = 0$ fs, the band at 586 cm^{-1} is the strongest and weak bands appear at 566, 313, and

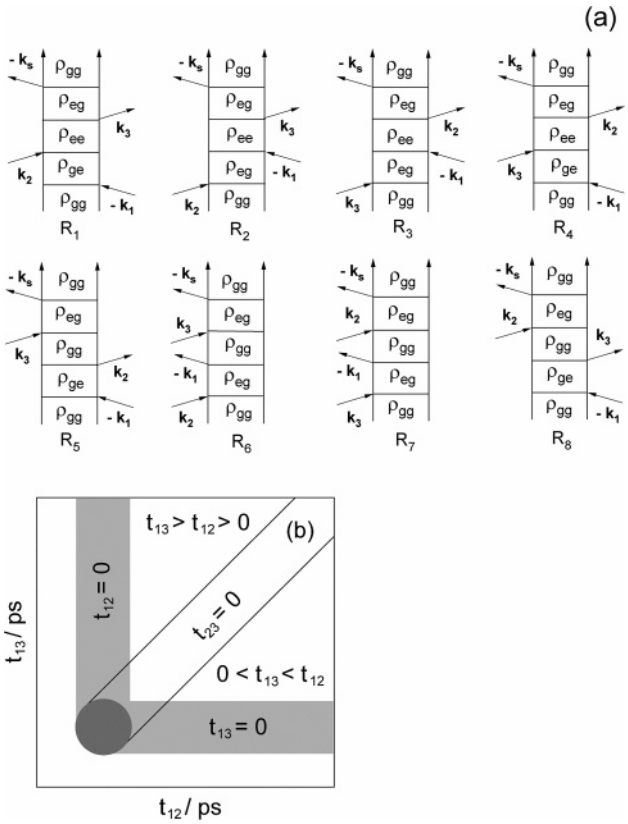

Figure 5. (a) Two-level system double-sided Feynman diagrams representing the evolution of the density matrix element for third-order nonlinear optical processes with phase-matching conditions of $-\boldsymbol{k}_1 + \boldsymbol{k}_2 + \boldsymbol{k}_3$. The left and right vertical lines represent the ket and bra of the density matrix, respectively. The time increases from bottom to top. The arrows on the left and right vertical lines represent the field−matter interactions on the ket and bra states. (b) Representative map of a two-dimensional plot of the DFWM signal against t_{12} and t_{13} showing the time ordering of pulse sequence. The contribution from the Liouville space pathways depends on the pulse sequence. For details, see the text. The denomination of the signal also depends on the pulse sequence. In the region where $t_{12} = 0$ or $t_{13} = 0$, the "transient grating" dominates the signal. The signal becomes equivalent to a "two-pulse photon echo" at $t_{23} = 0$, and the signal in the region for $t_{13} > t_{12} > 0$ or $t_{12} > t_{13} > 0$ is the "three-pulse stimulated photon echo" signal.

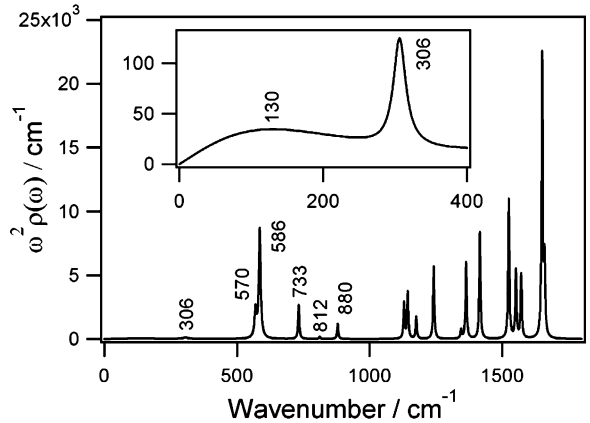

Figure 6. Model spectral density utilized for the computer simulation. The inset shows the lowest intramolecular band at 306 cm^{-1} with a broad Brownian oscillator peaked at 130 cm^{-1} which represents the phonon mode of the polymer glass.

270 cm^{-1}. For $t_{13} = 53$ fs, the bands at 313 and 270 cm^{-1} become comparatively strong and new bands appear at 33, 150, 228, and 351 cm^{-1}. The strongest band for $t_{13} = 107$ fs is the very broad band at ~33 cm^{-1}, and the band at 586 cm^{-1} still

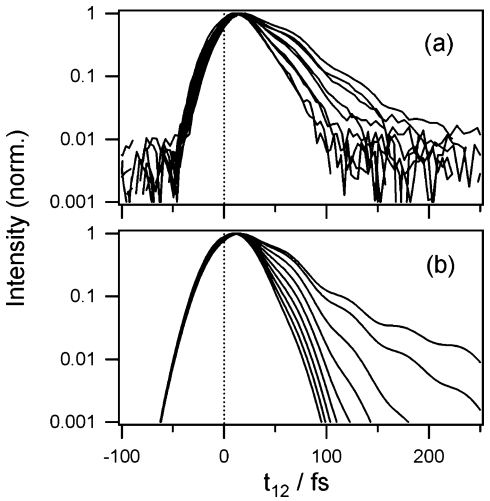

Figure 7. (a) Temperature dependence of the experimentally measured t_{12} dependence of the echo intensity generated from Ox4/PVA. The value of t_{23} was set at 387 fs. The echo decay slowed with decreasing temperature, and the temperature was set at 10, 30, 60, 90, 120, 150, 180, 210, and 240 K. (b) Calculated echo signal at the same temperatures.

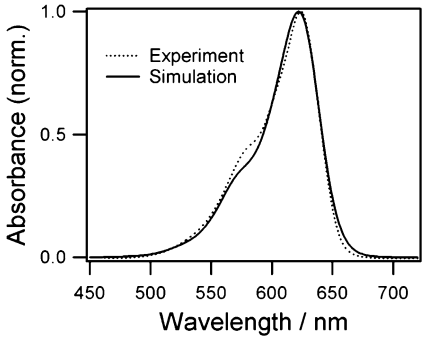

Figure 8. Experimentally measured spectrum of Ox4/PVA (dotted curve) and the one generated by the computer simulation (solid curve).

remains weakly, while the bands around 300 cm^{-1} have disappeared. The value of $t_{13} = 53$ fs corresponds to about half the oscillation period of the bands around ~300 cm^{-1} (*out of phase*), and these bands seem to be enhanced at this value of t_{13}. Note that such an enhancement effect was not observed for the band at 586 cm^{-1} for $t_{13} = 28$ or 85 fs which corresponds to one-half and three-halves of the oscillation period, respectively. A similar trend was also observed for Ox4/PMMA (Figure 3) and for Ox4 in glucose glass.[33] The reproducibility of the weak bands at 150, 228, and 351 cm^{-1} was confirmed.

Usually, for femtosecond time-domain measurements such as pump−probe and DFWM, the initial phases of oscillations are close to either 0 or π.[4] Therefore, the vibrational bands in the real part of the Fourier transformed spectrum have symmetric shapes, while those in the imaginary part have dispersive shapes. For the present experiment, the phase was nearly 0 at $t_{13} = 0$ fs and $t_{13} = 107$ fs. However, for $t_{13} = 53$ fs, a phase shift of about 15 fs was necessary to obtain symmetric band shapes in the real part of the spectrum. This shift can be observed in Figure 1b. We think that this shift is due to the convolution effect of the integrated echo signal.[29]

Although the signals of Ox4/PVA and Ox4/PMMA have similar features, there are some differences in detail. For example, at $t_{13} = 0$, the first peak is the strongest for the DFWM signal for Ox4/PMMA, while the second and third peaks are stronger for Ox4/PVA. The mode at 586 cm^{-1} is more strongly diminished at $t_{13} = 53$ fs for Ox4/PMMA than that for Ox4/PVA. The lowest frequency mode appears at ~15 cm^{-1} in PMMA, while it appears at ~33 cm^{-1} in PVA, respectively. The recurrence after the ultrafast decay is not very clear in PMMA compared to that in PVA, indicating that the mode has become more diffusive (exponential decay). The lowest frequency bands at 33 and 15 cm^{-1} are originating from the phonon mode of the polymer. These results indicate that dephasing may be slightly faster for Ox4/PMMA than that for Ox4/PVA owing to the slight difference in the coupling strength and/or in the frequency of the phonon mode.

Similar low-frequency coherent vibrations can be seen in the femtosecond pump−probe signal of Ox4/methanol solution at room temperature (Figure 4a).[24] The real part of the Fourier transformed spectrum is shown in Figure 4b, and four bands at 277, 306, 571, and 586 cm^{-1} can be seen, although other bands were not detectable. These bands can be assigned to the vibration in the ground state because they were also detected in the steady state resonance Raman spectrum.[22]

Our DFWM measurement at $t_{13} = 53$ fs was able to detect much weaker bands, which indicates that stimulated photon echo measurement could be a new method to enhance molecular vibrations. The signal at $t_{13} = 0$ fs corresponds to *in-phase* detection ($2\pi n/\omega$) with $n = 0$; thus, eq 1 suggests that coherent vibration in the TG signal is "suppressed" compared to that in the stimulated echo signal with an *out-of-phase* pulse sequence, that is, $t_{13} = 2\pi(n + 1/2)/\omega$.

Recently, Park and Joo have carried out a t_{12} dependent experiment of the TG signal generated from a dye, IR125, in methanol at room temperature.[34] Due to the ultrafast electronic dephasing in liquid, they could only change the value of t_{12} from −12 to 24 fs and the *out-of-phase* enhancement effect was not detectable. However, they succeeded in the observation of an enhancement or loss of the sharp feature in the signal near time zero, which is usually called "coherent spike". They also observed that the amplitude of the coherent oscillation was the strongest around $t_{12} = 12-16$ fs which was much shorter than the period of the oscillation they have observed, that is, ~200 fs. They concluded that this behavior is analogous to the control of the wave packets by controlling the chirp of the pump pulse.

3.2. Computer Simulations. To understand the experimental observations in detail, a computer simulation was carried out. When the laser pulses are sufficiently short and well separated with proper order, only two Liouville space pathways need to be concerned for the stimulated photon echo signal, which is represented by the double-sided Feynman diagrams R_1 and R_5 shown in Figure 5a. On the other hand, when pulses have a finite duration and the separation is insufficient, other pathways must be included.[20] The contribution from each pathway to the two-dimensional plot of the DFWM signal depends on the pulse sequence as depicted in Figure 5b. Near the time origin, $t_{13} = t_{12} = 0$, all eight pathways need to be considered. In the region where first and second pulses overlap, $t_{12} = 0$, the signal is dominated by the TG signal generated by the diffraction of the third pulse by the interferemetory pattern caused by the first and second pulses. In this region, the pathways that contribute are R_1, R_2, R_5, and R_6. In the region where the first and third pulses overlap, $t_{13} = 0$, the signal is dominated by the TG signal generated by the diffraction of the second pulse by the interferemetory pattern caused by the first and third pulses. In this region, the contributing pathways are R_3, R_4, R_7, and R_8. When the second and third pulses overlap, $t_{23} = 0$, the signal becomes equivalent to two-pulse photon echos and the contributing pathways are R_1, R_4, R_5, and R_8. Only in the region where $t_{13} > t_{12} > 0$, the signal can be ascribed as the ordinal stimulated

photon echo signal with pathways R_1 and R_5. For $0 < t_{13} < t_{12}$, an echolike signal is generated from rephasing pathways R_4 and R_8. Our measured signal lies in the region between $t_{13} = 0$ and $0 < t_{13} < t_{12}$. Therefore, the rephasing echolike contribution to our experimental signal mainly arises from pathways R_4 and R_8. To properly include such complicated contributions in the simulation, convolution analysis was applied.

The simulation was carried out according to the method described previously.[20,29,30,35] The echo signal was reconstructed starting from the model spectral density of the system shown in Figure 6. The line broadening function was calculated from the spectral density. Then, response functions for all the possible Liouville space pathways were calculated from the line broadening function. Finally, the photon echo signal was constructed from a convolution of the response functions with the laser pulses assuming a Gaussian shape with a fwhm of 26 fs.

The spectral density shown in Figure 6 was constructed from intramolecular vibrational modes of Ox4 and a phonon mode of the polymer. The parameters for intramolecular vibrations were taken from the steady state resonance Raman spectrum of Ox4.[22] The reorganization energy, λ_i, for the ith vibrational mode with a frequency of ω_i was calculated from the dimensionless displacements, D_i, listed in ref 22 using the relation $\lambda_i = \omega_i D_i^2/2$. Eighteen intramolecular modes were included in the spectral density. However, only the mode at 306 cm^{-1} was included below 400 cm^{-1} because the values of D_i for other modes were not available in this frequency region. The phonon mode of the polymer matrix was modeled by a Brownian oscillator[30]

$$C(\omega) = \frac{2}{\pi} \frac{\lambda_B \omega_B{}^2 \gamma_B}{(\omega_B{}^2 - \omega^2)^2 + \omega^2 \gamma_B{}^2} \qquad (2)$$

where λ_B, ω_B, and γ_B are the reorganization energy, frequency, and damping constant, respectively, which are the fitting parameters. The coupling to the component with an infinitively long decay time ($\gg$100 ps) was treated as the inhomogeneous (static) contribution, Δ_{in}, which is also a fitting parameter.

The fitting was first carried out on the temperature dependence of the echo signal of Ox4/PVA shown in Figure 7a. The data were taken by setting $t_{23} = 387$ fs and scanning t_{12} at temperatures of 10, 30, 60, 90, 120, 150, 180, 210, and 240 K. The value $t_{23} = 387$ fs was chosen because it is sufficiently long enough to avoid overlap of three pulses. Then, the absorption spectrum of Ox4/PVA shown in Figure 8 (dotted curve) was fitted. The parameters for the phonon mode in eq 2 are best obtained by fitting the temperature dependence of the echo signal, and the value of Δ_{in} is best obtained by fitting the absorption spectrum. This process was repeated until satisfactory fitting was achieved, and the results are shown in Figure 7b and in Figure 8 (solid curve). The detailed simulation was carried out only for Ox4/PVA. The four fitting parameters were determined to be $\lambda_B = 80$ cm^{-1}, $\omega_B = 210$ cm^{-1}, $\gamma_B = 400$ cm^{-1}, and $\Delta_{in} = 310$ cm^{-1}, respectively.

The phonon mode obtained from the simulation is shown in the inset of Figure 6, which peaks at 130 cm^{-1}. This peak frequency is much lower than the value $\omega_B = 210$ cm^{-1}, which is the result of a large damping constant, $\gamma_B = 400$ cm^{-1}. The temperature dependence of the calculated echo signal (Figure 7b) may be slightly exaggerated compared to the experimental result (Figure 7a). However, the level of the present simulation is sufficient enough for qualitative investigation of the coherent oscillation in the DFWM signal. The shoulder appearing around 580 nm in the experimental absorption spectrum (dotted curve in Figure 8) is reproduced by the simulation (solid curve), indicating that its origin is a vibrational structure and not an aggregate.

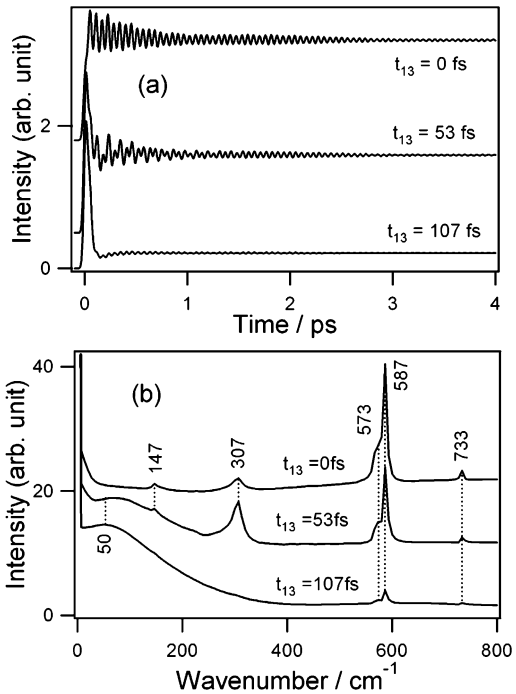

Figure 9. (a) Calculated DFWM signals of Ox4/PVA at different values of t_{13} at 10 K. (b) The real parts of the Fourier transformed spectra of the calculated signals.

The DFWM signals shown in Figure 9a were calculated from the obtained parameters. The simulation reproduced the experimental observations surprisingly well; the signal is oscillating at a lower frequency for $t_{13} = 53$ fs compared to $t_{13} = 0$ fs, and an ultrafast decay and a slight recurrence can be seen at $t_{13} = 107$ fs. There is a phase shift of about -7 fs at $t_{13} = 0$ fs and about $+5$ fs at $t_{13} = 53$ fs, while there was none at $t_{13} = 107$ fs.

The real parts of the Fourier transformed spectra of the calculated signals are shown in Figure 9b. Because we have included only one intramolecular mode at $<$400 cm^{-1} in the spectral density, only one band appears around 300 cm^{-1}. The intensity of this mode becomes stronger at $t_{13} = 53$ fs compared to $t_{13} = 0$ fs and disappears at $t_{13} = 107$ fs. The intensity of the strong band at 587 cm^{-1} just gradually decreases with increasing t_{13}, and it still remains weakly at $t_{13} = 107$ fs. Interestingly, a faint band can be seen at 147 cm^{-1} which we did not include in the spectral density. In the experimental data, a weak band at 147$-$150 cm^{-1} can be seen. This frequency corresponds to the difference between the band at 733 and 586 cm^{-1}. The appearance of a difference frequency band was also reported for the echo experiment and simulation of Nile blue in room temperature solvents.[36,37] At $t_{13} = 53$ fs, a low-frequency mode at $\sim$67 cm^{-1} appears and increases its intensity and shifts down to $\sim$50 cm^{-1} at $t_{13} = 107$ fs. This frequency is slightly higher than the observed frequency of $\sim$30 cm^{-1}. The origin of the low-frequency band is indeed the phonon mode of the polymer; however, it should be noted that the frequency obtained from the DFWM signal (50$-$67 cm^{-1}) does not directly reflect the actual frequency of the phonon mode (130 cm^{-1} in Figure 6). At this point, it is not obvious why only the lower frequency portion of the overdamped phonon mode contributes to the decay of the signal at small values of t_{13} and further investigation is

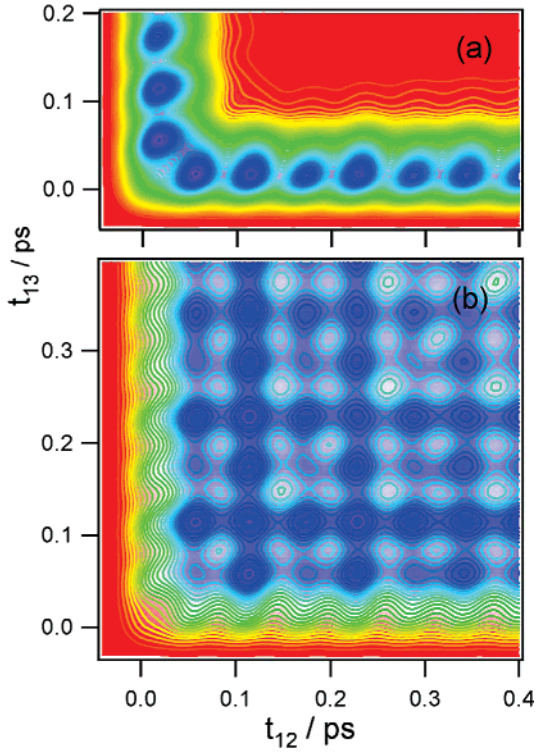

Figure 10. (a) Two-dimensional plot of the calculated DFWM signal of Ox4/PVA at 10 K. (b) Two-dimensional plot of the calculated DFWM signal at 10 K with the reorganization energy, λ_B, for the phonon mode set to zero.

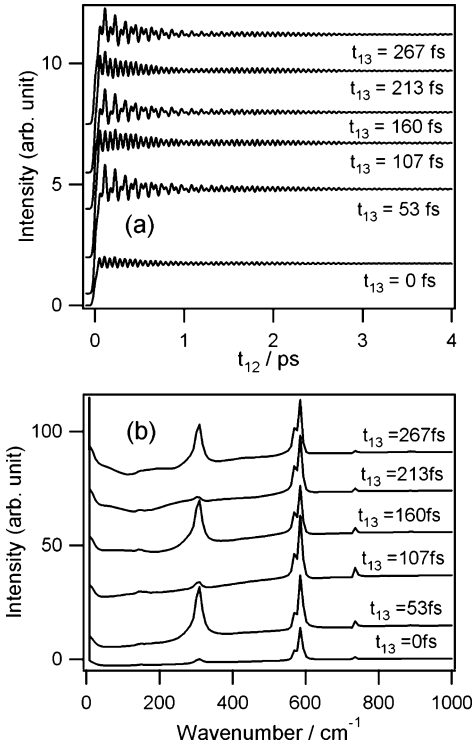

Figure 11. (a) Calculated DFWM signals at different values of t_{13} at 10 K with $\lambda_B = 0$. (b) The real parts of the Fourier transformed spectra of the calculated signals with $\lambda_B = 0$.

necessary. For the very-low-frequency mode, there is a possibility of an enhancement effect other than that represented by eq 1.

Figure 10a is the two-dimensional plot of the entire calculated signal. In the range where t_{12} and t_{13} are much larger than 0, the signal intensity is reduced to zero, as observed in the experimental result shown in Figure 1a. This is due to the ultrafast dephasing caused by the coupling to the polymer phonon mode. If we could reduce the contribution from the phonon mode, the coherent oscillation can be investigated in a wider time range. While this was not possible in the present experiment, the coupling can be reduced to zero in the simulation.

Figure 10b shows the 2D plot of the calculated signal with coupling to the phonon mode reduced to zero ($\lambda_B = 0$). It can be seen that the dephasing time has elongated and a strong signal is still present in the range of $t_{12} \gg 0$ and $t_{13} \gg 0$. In Figure 11a, it is shown that the dependence of the signal intensity on t_{12} changes regularly with the value of t_{13} with a period of ~53 fs. There was a phase shift of about −7 fs at $t_{13} = 0$ fs, while it was zero at other values of t_{13}. Fourier transform was applied to the signal, and the real parts of the spectra are shown in Figure 11b. The low-frequency band at 67−50 cm^{-1} is no longer present because there is no coupling to the phonon mode. The band at 306 cm^{-1} periodically changes its intensity in an *out-of-phase* manner with its own period. This dependence is similar to the one predicted by eq 1. Note that the amplitude of the oscillation is actually enhanced when the delay is set *out of phase* with the vibration. On the contrary, the intensity of the strong band at 586 cm^{-1} stays rather constant and it did not reveal any noticeable dependence on the phase.

To explore the different dependence on t_{13} between the bands at 306 and 586 cm^{-1}, further simulation was carried out. In Figure 12a, all the reorganization energies for the bands below

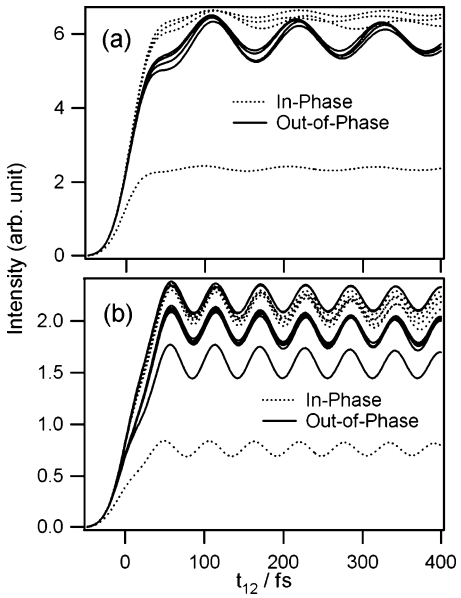

Figure 12. (a) Calculated DFWM signals at different values of t_{13} at 10 K with all the reorganization energies for the bands below 800 cm^{-1} set to zero except the band at 307 cm^{-1}. The signal with the weakest intensity corresponds to $t_{13} = 0$, and other signals are calculated by increasing the value of t_{13} with a step of 53 fs up to 371 fs. The dotted curve represents the *in-phase* signal, and the solid curve represents the *out-of-phase* signal, respectively. (b) Calculated stimulated echo signals at different values of t_{13} at 10 K with all the reorganization energies for the bands below 800 cm^{-1} set to zero except the band at 586 cm^{-1}. The signal with the weakest intensity corresponds to $t_{13} = 0$, and other signals are calculated by increasing the value of t_{13} with a step of 28 fs up to 392 fs.

800 cm^{-1} were set to zero except the band at 306 cm^{-1}, and the dependence of the DFWM signal on t_{12} was calculated by increasing the value of t_{13} with a step of 53 fs. The signal with

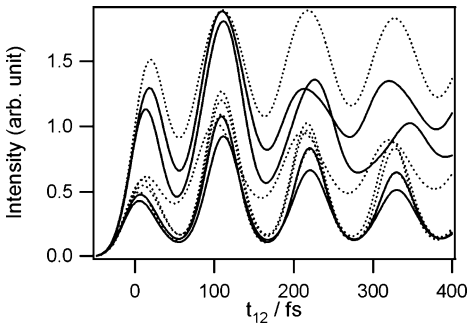

Figure 13. Calculated DFWM signals at different values of t_{13} at 10 K with all the reorganization energies for the bands below 800 cm^{-1} set to zero except the band at 307 cm^{-1}. The reorganization energy for this band was increased to 188 cm^{-1}. The signals were calculated by increasing the value of t_{13} with a step of 53 fs from 0 to 371 fs. The dotted curve represents the *in-phase* signal, and the solid curve represents the *out-of-phase* signal.

the lowest intensity is the one at $t_{13} = 0$. It can be clearly seen that the amplitude of the oscillation increases when the delay is set *out of phase* with the vibrational period which is consistent with eq 1. On the other hand, when the signal was calculated with only the band at 586 cm^{-1} left in the region of <800 cm^{-1} (Figure 12b), no noticeable phase dependence was observed. In Figure 12b, the dependence of the signal on t_{12} was calculated by increasing the value of t_{13} with a step of 28 fs starting from $t_{13} = 0$. The amplitude of the oscillation was similar with t_{13} set to either *in phase* or *out of phase* with the vibration.

The bands at 306 and 586 cm^{-1} differ not only in frequency but also in coupling strength. The reorganization energy, λ_i, for the band at 586 cm^{-1} is 188 cm^{-1} which is more than 15 times larger than the one at 306 cm^{-1} which is only 11 cm^{-1}. To elucidate the effect of the coupling strength on the coherent oscillation, the DFWM signal was calculated with $\lambda_i = 188$ cm^{-1} for the band at 306 cm^{-1}, while λ_i for other bands below 800 cm^{-1} were set to zero. The results are shown in Figure 13, and the oscillation became fierce and the difference between *in phase* (dotted curve) and *out of phase* (solid curve) is not clear any more. It can be concluded that the enhancement effect is only observable for low-frequency modes with small reorganization energies.

4. Concluding Remarks

The DFWM experiment on Ox4 in polymer films at 10 K revealed that the intensities of some low-frequency coherent vibrations around 300 cm^{-1} were enhanced for the stimulated photon echo signal at $t_{13} = 53$ fs compared to those in the transient grating signal at $t_{13} = 0$ fs. A strong and broad low-frequency mode at <40 cm^{-1} was also present for $t_{13} > 0$ fs which originates from the phonon mode of the polymer; however, the peak frequency of this mode is not directly related to that of the phonon mode. Computer simulation based on the evolution of density matrix formalism in Liouville space, which assumes linear electronic coupling to the harmonic spectral density, reproduced the experimental result successfully. It was indicated that the intensity of the low-frequency mode with small reorganization energy can be enhanced by setting t_{13} *out of phase* with the oscillation. Such an enhancement effect can be applied to the study of weak low-frequency modes such as intermolecular vibrations between substrates and adsorbates or charge-transfer complexes.

Acknowledgment. This research was supported partly by a Grant-in-Aid for Exploratory Research (no. 14654104), Specially Promoted Research (no. 10102007), and Research in Priority Area (no. 432) from the Ministry of Education, Culture, Sports, Science and Technology of Japan, and the development of the Cr:F laser was partially supported by Sumitomo Foundation. Y.N. wants to thank Prof. T. Joo for providing the original code for the computer simulation and also Prof. T. Tahara for fruitful discussions.

References and Notes

(1) Dhar, L.; Rogers, J. A.; Nelson, K. A. *Chem. Rev.* **1994**, *94*, 157.
(2) Zewail, A. H. *J. Phys. Chem.* **1996**, *100*, 12701.
(3) Harris, A. L.; Brown, J. K.; Hariis, C. B. *Ann. Rev. Phys. Chem.* **1988**, *39*, 341.
(4) Jonas, D. M.; Fleming, G. R. Vibrationally abrupt pulses in pump−probe spectroscopy. In *Ultrafast prcesses in photochemistry and photobiology*; E1-Sayed, M., Tanaka, I., Y., M., Eds.; Blackwell Scientific: Oxford, U.K., 1995; p 225.
(5) Vos, M. H.; Martin, J.-L. *Biochim. Biophys. Acta* **1999**, *1411*, 1.
(6) Vos, M. H.; Rappaport, F.; Lambry, J.-C.; Breton, J.; Martin, J.-L. *Nature* **1993**, *363*, 320.
(7) Kobayashi, K.; Saito, T.; Ohtani, H. *Nature* **2001**, *414*, 531.
(8) Dantus, M.; Lozovoy, V. V. *Chem. Rev.* **2004**, *104*, 1813.
(9) Assion, A.; Baumert, T.; Bergt, M.; Brixner, T.; Kiefer, B.; Seyfried, V.; Strehle, M.; Gerber, G. *Science* **1998**, *282*, 919.
(10) Brixner, T.; Damrauer, N. H.; Niklaus, P.; Gerber, G. *Nature* **2001**, *414*, 57.
(11) Jonas, D. M. *Ann. Rev. Phys. Chem.* **2003**, *54*, 425.
(12) Khalil, M.; Demirdoven, N.; Tokmakoff, A. *J. Phys. Chem. A* **2003**, *107*, 5258.
(13) Asplund, M. C.; Zanni, M. T.; Hochstrasser, R. M. *Proc. Natl. Acad. Sci. U.S.A.* **2000**, *97*, 8219.
(14) Bredenbeck, J.; Helbing, J.; Hamm, P. *J. Am. Chem. Soc.* **2004**, *126*, 991.
(15) Zhao, W.; Wright, J. C. *Phys. Rev. Lett.* **1999**, *83*, 1950.
(16) Khalil, M.; Demirdoven, N.; Tokmakoff, A. *Phys. Rev. Lett.* **2003**, *90*, 047401.
(17) Brown, E. J.; Pastirk, I.; Grimberg, B. I.; Lozovoy, V. V.; Dantus, M. *J. Chem. Phys.* **1999**, *111*, 3779.
(18) Grimberg, B. I.; Lozovoy, V. V.; Dantus, M.; Mukamel, S. *J. Phys. Chem. A* **2002**, *106*, 697.
(19) Narasimhan, L. R.; Littau, K. A.; Pack, D. W.; Bai, Y. S.; Elschner, A.; Fayer, M. D. *Chem. Rev.* **1990**, *90*, 439.
(20) Joo, T.; Jia, J.; Yu, J.-Y.; Lang, M. J.; Fleming, G. R. *J. Chem. Phys.* **1996**, *104*, 6089.
(21) de Boeij, W. P.; Pshenichnikov, M. S.; Wiersma, D. A. *J. Phys. Chem.* **1996**, *100*, 11806.
(22) Bardeen, C. J.; Rosenthal, S. J.; Shank, C. V. *J. Phys. Chem. A* **1999**, *103*, 10506.
(23) Vöhringer, P.; Arnett, D. C.; Yang, T.-S.; Scherer, N. F. *Chem. Phys. Lett.* **1995**, *237*, 387.
(24) Nagasawa, Y.; Watanabe, A.; Takikawa, H.; Okada, T. *J. Phys. Chem. A* **2003**, *107*, 632.
(25) Bardeen, C. J.; Cerullo, G.; Shank, C. V. *Chem. Phys. Lett.* **1997**, *280*, 127.
(26) Bardeen, C. J.; Shank, C. V. *Chem. Phys. Lett.* **1993**, *203*, 535.
(27) Schoenlein, R. W.; Mittleman, D. M.; Shiang, J. J.; Alivisatos, A. P.; Shank, C. V. *Phys. Rev. Lett.* **1993**, *70*, 1014.
(28) de Boeij, W. P.; Pshenichnikov, M. S.; Wiersma, D. A. *J. Chem. Phys.* **1996**, *105*, 2953.
(29) Nagasawa, Y.; Seike, K.; Muromoto, T.; Okada, T. *J. Phys. Chem. A* **2003**, *107*, 2431.
(30) Mukamel, S. *Principles of Nonlinear Optical Spectroscopy*; Oxford University Press: New York, 1995.
(31) Nagasawa, Y.; Ando, Y.; Watanabe, A.; Okada, T. *Appl. Phys. B* **2000**, *70* (Suppl.), S33.
(32) Matsuda, H.; Nagasawa, Y.; Miyasaka, H.; Okada, T. *J. Photochem. Photobiol., A* **2003**, *156*, 69.
(33) Nagasawa, Y.; Ogasawara, M.; Nakagawa, Y.; Mori, Y.; Okada, T.; Miyasaka, H. *Ultrafast Phenomena XIV*; Kobayashi, T., Okada, T., Kobayashi, T., Nelson, K. A., De Silvestri, S., Eds.; Springer-Verlag: Berlin, 2005; p 598.
(34) Park, J.-S.; Joo, T. *J. Chem. Phys.* **2004**, *120*, 5269.
(35) Nagasawa, Y.; Passino, S. A.; Joo, T.; Fleming, G. R. *J. Chem. Phys.* **1997**, *106*, 4840.
(36) Larsen, D. S.; Ohta, K.; Xu, Q.-H.; Cyrier, M.; Fleming, G. H. *J. Chem. Phys.* **2001**, *114*, 8008.
(37) Ohta, K.; Larsen, D. S.; Yang, M.; Fleming, G. R. *J. Chem. Phys.* **2001**, *114*, 8020.